

Mitigation of Reflected Shock Wave by Streamwise Plasma Array

*Sergey Leonov**, *Campbell Carter***, *Alec Houpt**, and *Timothy Ombrello***

**Institute for Flow Physics and Control, University of Notre Dame*

Notre Dame, IN, 46556, USA (Leonov.1@nd.edu)

*** U.S. Air Force Research Laboratory*

Wright-Patterson AFB, OH, 45433, USA

Abstract

This work focuses on the results of an experimental study of the Quasi-Direct-Current (Q-DC) electrical discharge impact on the shock-wave structure and wall-pressure distribution in a supersonic duct-driven airflow. A major attention is paid for the effect of plasma streamwise array on a reflection pattern of the impinging shock wave at interaction with the boundary layer.

1. Introduction

The control of shock wave (SW) interaction with a boundary layer (BL), other SWs, and separated flows in a supersonic/hypersonic airflow is of fundamental and technological interest for aerospace science and industry. Currently airflow conditioning in supersonic inlets is one of the major issues of high-speed airbreathing propulsion, [1,2,3,4] and references herewith. The flow structure in the duct (isolator), at the entrance to the combustor, at the compression surfaces of the inlet, and over other control surfaces is sensitive to the geometrical configuration and main flow parameters, including the state of the boundary layer and the presence of compression/expansion waves previously impinging the BL. In most cases the control schemes include stationary / movable mechanical elements or gas wall jets. Problems here are in a lack of flexibility, a total pressure loss, and frequently in a long response time, orders of magnitude longer than a characteristic gasdynamic time.

Intensive studies of the physical processes of supersonic / hypersonic shock wave - boundary layer interaction (SWBLI) have been motivated by the needs of scramjet systems for air-breathing vehicles. For airframe-integrated scramjet engines, the forebody ahead of the inlet is designed to process and pre-condition the flow that will be ingested by the air inlet. The flow conditioning is frequently desirable at the entrance to the inlet to mitigate flow separations on compression ramps and prevent air inlet unstarts [5,6]. It was suggested that the most effective tripping mechanism requires the formation of streamwise vorticity within the boundary layer [7,8]. In addition to mechanical tripping, a thermal type of boundary layer management was demonstrated to be feasible [9]. The mechanical elements or steady-state thermal sources produce stationary forcing of the flow generating steady-state SWs with a predefined location. It is reasonable to assume that unsteady forcing, which generates disturbances of the required length-scale and frequency, may be much more effective. Such an unsteady forcing can be produced by synthetic jets, laser pulses, and/or plasma actuators. The dynamics of the artificially induced highly transient disturbances recently attracted attention [10,11,12] but has not yet been studied in full detail.

The importance of plasma non-uniformity and its transient behavior for SW and boundary layer control has been considered in numerous publications [13,14,15,16,17,18]. Localized heating generated by the plasma may produce "hot spots" operating similar to solid obstacles, although this interpretation may well be too simplistic. The flow interaction with the hot spots may result in a generation of new flow structures, such as streamwise vortices and wavelets convecting with the flow, while a rapid modulation of discharge energy coupling / body force may lead to tripping the boundary layer. In Ref. [13], a transient growth of boundary layer perturbations was demonstrated using a spanwise array of plasma actuators. In this work, plasma actuators have been used to reduce the energy of perturbations generated by surface roughness, by up to 70%, in three different geometries. In Ref. [14], plasma actuator control of the boundary layer separation on the leading edge of an airfoil has been demonstrated for free stream velocities up to 93 m/s and Reynolds numbers up to 1.15×10^6 . It was concluded that the flow control mechanism is due to excitation of shear layer instabilities by rapid localized heating of flow near the surface. Finally, pulse-periodic localized heating by different types of electric discharges has been used for jet noise reduction in Ref. [16]. Another group of plasma-related studies is focused on high-speed applications [19,20,21]. Repetitive thermal perturbations have been applied

for high-speed flow control using phased arrays of repetitively pulsed Localized Arc Filament Plasma Actuators (LAFPAs), generating small scale, pulsed DC filament discharges between pairs of pin electrodes ~ 1 mm apart, flush mounted in a nozzle wall [20,22,23,24]. The main premise of this approach was forcing the flow with a high amplitude perturbation, at a frequency approaching one of the flow instability frequencies, triggering their subsequent growth in the flow. LAFPA flow control experiments in atmospheric pressure jet flows ($M=0.9-2.0$) demonstrated significant localized heating in the near-surface discharge filaments [25] and repetitive compression wave formation by the plasma [24]. In addition to this, LAFPA actuators also excite flow instabilities, generate large-scale coherent structures in the flow [23,26], and result in significant mixing enhancement and shear layer properties [27].

It is well known that intense, localized, rapid heating produced by plasmas in high-current pulsed electric discharges (similar to pulsed optical discharges) produce strong shock waves, which can considerably modify supersonic flows. Basically, rapid near-adiabatic heating results in an abrupt pressure jump in the current filament. The plasma-based technique was explored in terms of the feasibility of steady or transient shock wave (SW) generation in supersonic flow [28,29,21]. This suggests that rapidly heated regions located near aerodynamic surfaces could be used to control the pressure distribution in a variety of aerodynamic configurations. To some extent, they operate similar to mechanical apparatuses of appropriate shape, simulating a *virtual aerodynamic shape*. The *virtual aerodynamic shape* is a figurative shape of a contoured body providing the flow pattern similar to that which is produced by a physical shape inserted into the flow. The *virtual aerodynamic shape* is generated using a mass or energy addition to the flowfield. In this meaning, the term was first used in Ref. [30].

This work is aimed at the study of shock wave - boundary layer interaction, surface pressure redistribution on a plane wall, and dynamics of the airflow structure under the impact of on-surface generated, transient energy deposition in a shock-dominated airflow. An instant power deposition into the gas is provided by means of a Quasi-DC electrical discharge, which generates a filamentary plasma between flush mounted surface electrodes with a crossflow orientation. Due to the unsteady behavior of the individual plasma filaments, this type of electrical discharge was called a “Quasi-DC” or Q-DC discharge [31,32].

Developing appropriate plasma-based flow control techniques may result in numerous potential applications. Despite a large interest in this scientific field the feasibility and the efficiency of practical implementation remains unclear. One of the important goals of this work is to determine the benefits and drawbacks of the plasma-based approach for SWBLI control in supersonic / hypersonic flow.

2. Test facility, instrumentation and Q-DC discharge characterization.

The experiments were performed in the supersonic blow-down wind tunnel SBR-50. The test section is arranged inline with a Mach 2 Laval nozzle. The cross section at the exit of the nozzle ($x=0$) is $Y \times Z = 76.2$ mm (width) \times 76.2 mm (height), with a 1° expansion angle and a total length of $x = 610$ mm measured to the diffuser, as it is shown in Fig. 1. The electrical discharge generators are flush-mounted on a plane wall as a single unit, indicated in Fig.1 as “PA” – Plasma Array. The test section of the SBR-50 high-speed facility is equipped with 2 pairs of quartz windows placed as the side walls of the duct for optical access. In the current experimental series the conditions were as follows: initial Mach number $M=2$; total pressure $P_0 = 1-2.2$ bar; stagnation temperature $T_0 = 300$ K; duration of steady-state aerodynamic operation $t = 1-2$ s. A trail of reflecting shock waves, related to the plasma generation, is indicated by straight lines. Figure 2a shows the plasma array schematics. Instrumentation available for the current tests include:

- pressure distribution, 48 pressure ports over the top and bottom walls, 16 channels PSI 9116 scanner, response time 2.5ms;
- fast camera imaging Photronic FastCam (b/w) and Casio EX-FH100 Camera (color);
- high-definition schlieren system, details are described in [32];
- optical emission spectroscopy (OES);
- set of electrical probes.

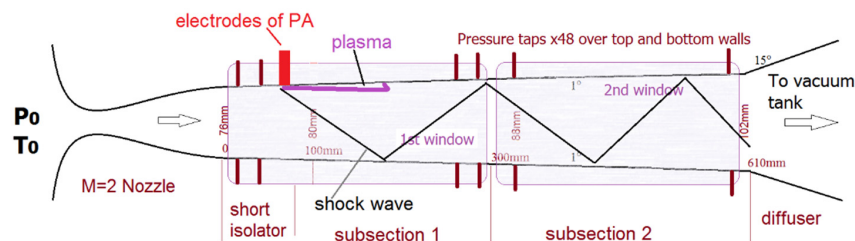


Figure 1. Geometrical configuration of the SBR-50 test section.

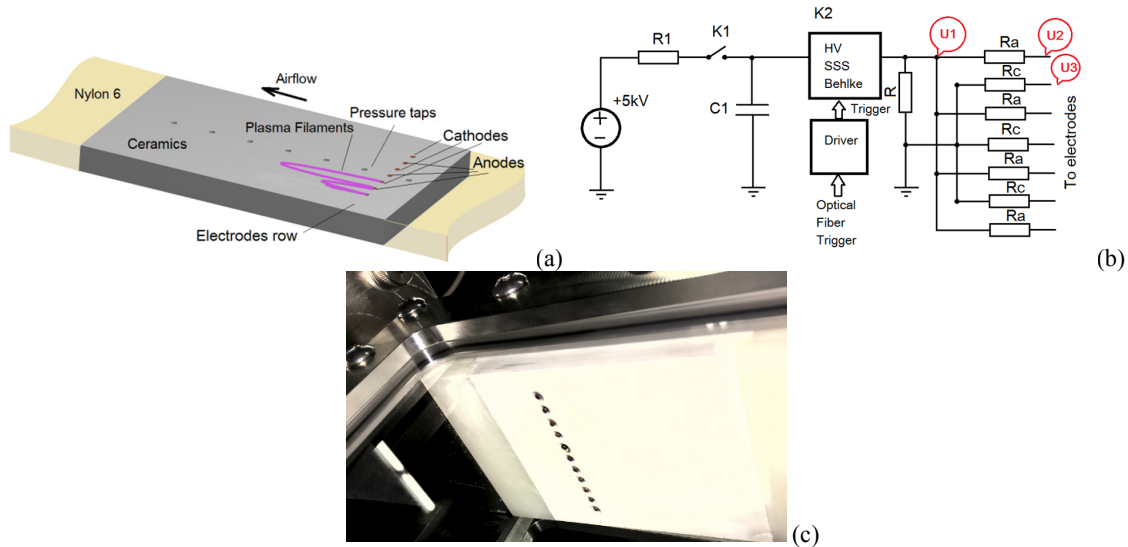


Figure 2. Plasma generator arrangement: (a) electrode arrangement; (b) electrical schematics; (c) photo of the plasma array with 11 electrodes mounted in the test section.

The custom-made power supply used in the present experiments is designed to operate with a steep falling voltage-current characteristic and individual control of each output channel as it is shown in Fig.2b. The electrodes were powered by a constant-voltage, $U_{ps}=5$ kV. The power supply has been connected to the electrodes with the help of a solid-state Behlke™ switch (K2 shown in Fig.2b). In this test series, the geometry included 7 electrodes: 4 cathodes + 3 anodes or 11 electrodes: 6 cathodes + 5 anodes, as it is shown in Fig.2c. The cathodes and anodes are alternated along the electrode row in such a way that the adjacent electrodes are connected to the high-voltage side (anodes) and to the grounded side (cathodes). The ballast resistors normally used are $R_a=0.5-1$ kOhm and $R_c=0.1-0.2$ kOhm. Voltages $U1$ to $U3$ characterized values at the power supply exit $U1$, the voltage at the anode $U2$ and the voltage at the cathode $U3$, as well as the voltage on the plasma gap $U_{pl}=U2-U3$, electric current through a cathode $I_{plc}=U3/R_c$, and electric current through an anode $I_{pla}=(U1-U2)/R_a$. These data then were compared to the total plasma current I_{pl} via the Pearson™ current probe and to derive the total plasma power deposition $W_{pl}\approx U_{pl}\times I_{pl}$. Typical discharge parameters were as follows: electrode spacing $L_0=5-8$ mm, average current through all electrodes $I_{pl}=10-25$ A; voltage across the gap $U_{pl}=500-1200$ V; average power coupled per unit spanwise distance $W_{pl}/Z=0.5-3$ kW/cm; duration of plasma operation $t_{pl}=10-300$ ms, which is much longer than a characteristic gas dynamic time $t_{gd}=D/V\approx 0.2$ ms, where $D\approx 10^{-1}$ m is a characteristic length corresponding to the maximum length of plasma filaments and $V\approx 500$ m/s is the core flow velocity. Time sequences of $U1-U3$ voltages, plasma voltage, and the discharge power are shown in Fig.3 gathered at a static pressure $P_{st}=0.4$ bar and a total plasma power release $W_{pl}\approx 20.2$ kW. A strong coupling of the plasma to the flowing gas causes fast oscillations of the plasma shape, and consequently, of the plasma voltage and power, as shown in Fig.4b. The saw-tooth waveform of the plasma voltage [32] is a result of the movement of individual plasma filaments with the airflow.

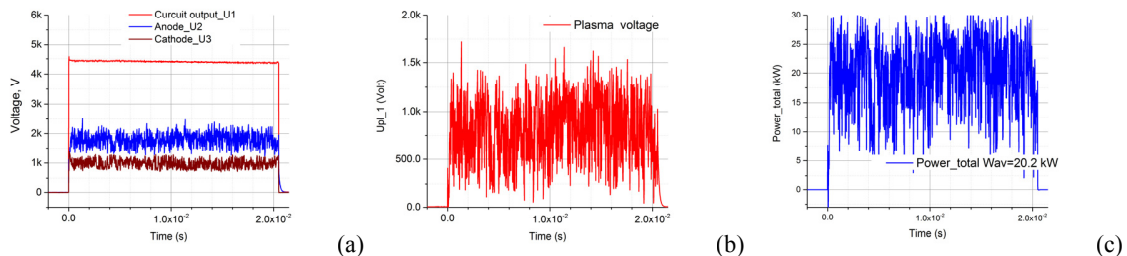


Figure 3. Typical voltage-power record: (a) voltage traces $U1$, $U2$ and $U3$; (b) voltage on electrode gap U_{pl} ; (c) discharge power recalculated W_{pl} .

The plasma shape appears in the form of a loop of a constricted (filamentary) plasma connecting the neighboring electrodes as shown in the images in Fig.4. The discharge dynamics are described in the following way. In the

beginning of the plasma filament development, breakdown occurs across the flow between the high-voltage electrodes and the grounded electrodes through the shortest distance. Next, the plasma filaments are transported by the flow and extend downstream over a distance up to 50-100 mm while remaining close to the surface of the ceramic insert. Very often the individual shape of a plasma filament remains similar for a long time, up to 100 μ s, elongating downstream with a more or less constant speed. When a plasma loop achieves a critical length a new breakdown occurs somewhere upstream, between the longitudinal portions of the plasma filaments; consequently, the location of the filaments and the discharge voltage oscillates at a frequency of several kilohertz. The dominant frequency of oscillations is $F=8-15$ kHz, depending on the inter-electrode gap and the gas density / velocity, that is resulted from the difference in the plasma loop lengths. This is demonstrated in Figs. 4 and 5 where the plasma filaments are shorter for the 11 electrode discharge than for the 7 electrodes case. Figure 5 presents a longitudinal distribution of the plasma luminosity along the filaments for both cases and variation of the gas pressure indicating a significantly different shape of the plasmas especially for a lower pressure case. At lower pressures the 11 electrode discharge oscillates at a higher frequency, as it is shown in Fig.6a. As the pressure increases the dominant frequency of the 11 electrode array approaches that of the 7 electrode array. The discharge is not only coupled to the flow through oscillations, the power released to the plasma is dependent on the resistors installed in the circuit, velocity, and static pressure. The plasma power is typically in the range of 5-20 kW for the parameters used for this work. Figure 6b shows the nearly linear dependence of the power on the static pressure when the circuit parameters/geometry are held constant. It is important to note that at the same average current the power release for the 11 electrode configuration is significantly lower than for the 7 electrode pattern.

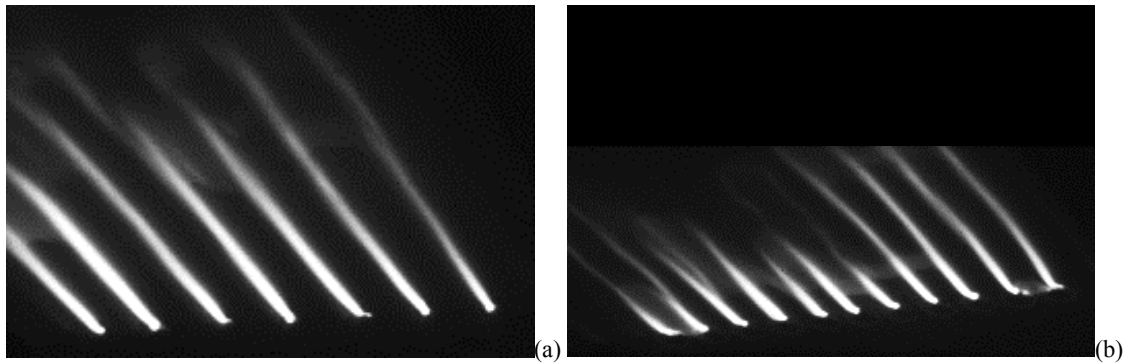


Figure 4. Images of the Q-DC plasma at $P_{st}=270$ mbar: (a) 7 electrode configuration; (b) 11 electrode configuration.

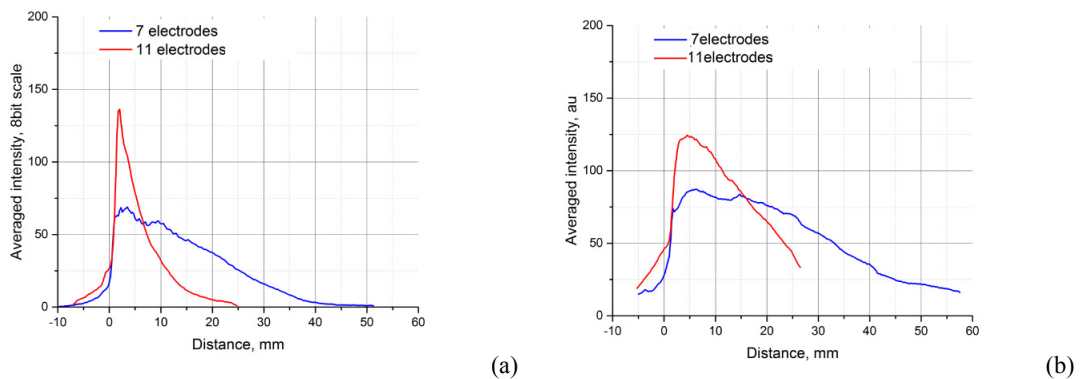


Figure 5. Average pixel intensity from image processing for 7 electrode vs 11 electrode configuration: (a) $P_{st}=120$ mbar; (b) $P_{st}=270$ mbar.

MITIGATION OF REFLECTED SHOCK WAVE BY STREAMWISE PLASMA ARRAY

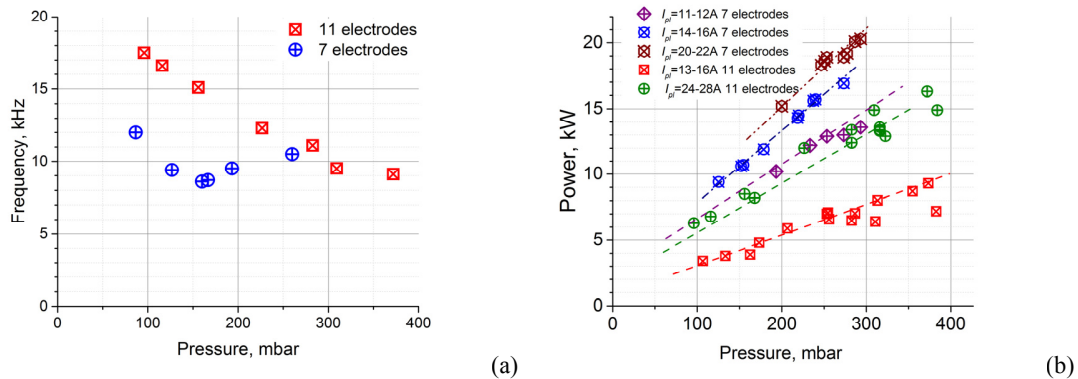


Figure 6. Data for discharge oscillation frequency (a) and plasma power (b) as a function of discharge arrangement, electrical current, and static pressure.

Optical emission spectroscopy was used to measure the plasma temperature. The discharge luminescence was collected from the discharge zone using a circular area with a diameter of $d \approx 10$ mm located downstream of the HV electrode in the distance range $x \approx 10 - 120$ mm at an airflow pressure $P_{st} = 250$ mbar and plasma power $W_{pl} = 18$ kW. Spectral fitting of the well-resolved band returns the range of translational and vibrational gas temperature: $T_{tr} = T_v = 6300 \pm 300$ K, $T_v = 10000 \pm 1000$ K [32]. Note that these values are related to the plasma zone with the maximum electron temperature. With a high local gas temperature, the multi-filamentary plasma zone presents an array of longitudinal subsonic jets surrounded by a supersonic flow. The volumetrically expanded zone produces a long cone of subsonic flow, where the physical velocity may be close to the gas speed in the supersonic core flow. Such an uncommon gasdynamic structure produces a near-surface stratified zone which enables a significant redistribution of the gas pressure. The shock wave interaction with a single heated filament has been explored numerically [33,34] but the SW-array interaction did not have proper experimental evidence until now.

3. Experimental results

The effect of the Q-DC plasma generated near the plane wall consists of gas heating in the airflow zone downstream of the electrode system, which causes an increase of the gas pressure and the subsequent propagation of a compression wave. In supersonic airflow, an oblique shock wave (SW) is observed originating from the root part of the plasma filaments, as it is shown in schlieren image Fig. 7. The SW impinges on the opposite (bottom) wall increasing the pressure in the zone of interaction. Then, a series of SW reflections is observed in the test section downstream of the plasma generator, see Fig. 1. Also, Figure 7 shows an important feature of the Q-DC generated shock wave; despite the filamentary and transient nature of the discharge the generated shockwave is planar in the region away from the electrodes.

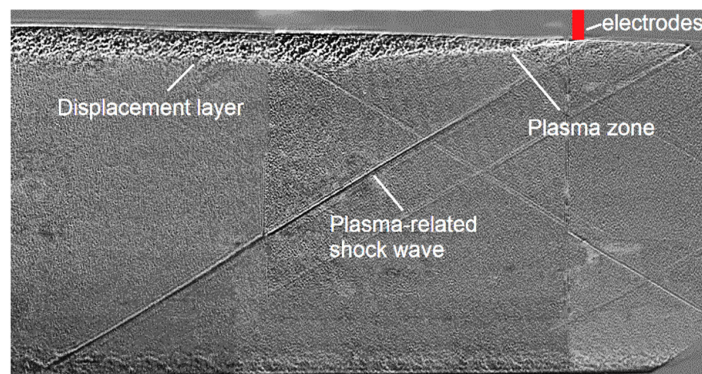


Figure 7. Effect of Q-DC electrical discharge on supersonic flow: schlieren image of flow structure at plasma generation; flow is from right to left.

The 16 channel pressure transducer provides the dataset of pressure distribution throughout the test section. The pressure distribution for the wall opposite the electrodes is presented in Fig. 8 for the 7 and 11 electrode discharges. In Fig. 7a and 7b there are two large pressure increases which occur at approximately 140 mm and 400 mm. These

pressure peaks are a result of the shock wave-boundary layer interaction between the plasma generated shock wave and the opposite wall. The area influenced by the 7 electrode discharge is much larger than that influenced by the 11 electrode discharge. The relative pressure increase (maximum pressure increase normalized by the static pressure at that point) without the discharge for both arrays is shown in Fig. 8. The pressure increase as a function of plasma power for 7 and 11 electrodes follow the same linear trend. Therefore the 7 and 11 electrode arrays should have similar effects on the pressure rise holding plasma parameters equal. This data reveals that the 11 electrode system can target a smaller area of influence while achieving the same relative pressure increase.

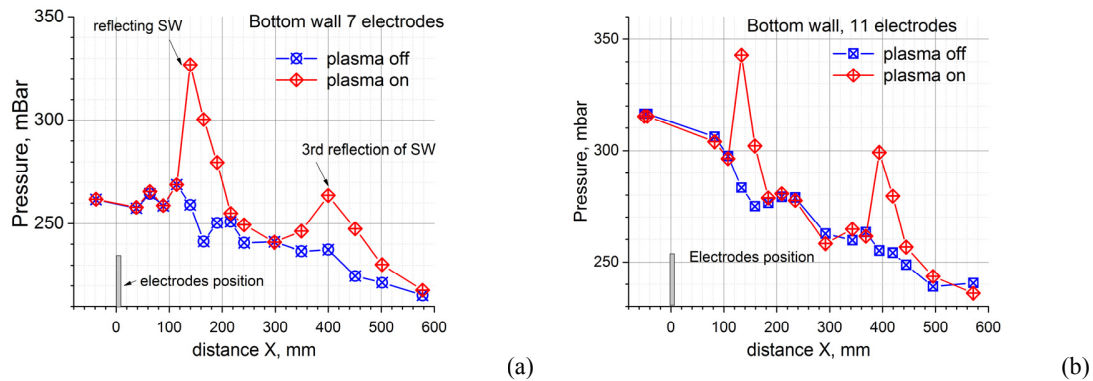


Figure 7. Pressure distributions over the wall opposite the electrodes for (a) 7 electrodes and (b) 11 electrodes.

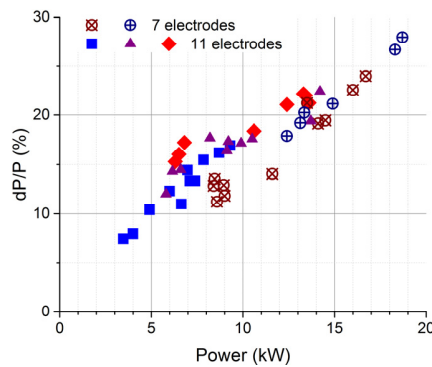


Figure 8. Amplitude of relative pressure increase as a function of plasma power.

Summarizing the basic effect of the plasma on the flowfield, three simple rules are realized as follows: (1) a higher angle of the plasma-related shock wave is observed at greater plasma power; (2) a higher pressure elevation on the opposite wall is observed at greater plasma power; and (3) a relative pressure augmentation is a conservative function of the gas pressure within the same parameters of the electrode system / power supply but rises with an increase of the discharge power.

The experiments were performed to explore the pattern of oblique shock wave - plasma layer interaction in the presence of a fixed SW generator. A 50 mm long solid wedge was installed on the opposite wall of the test section, as it is seen in Figs. 9 and 11. The angle was variable in a range of 3-9°. The tests were made using the plasma power range $W_{pi}=16-18\text{kW}$; initial static pressure $P_{st}=280-300\text{ mbar}$. The result of the interaction for the 3° wedge is shown in Figs. 9 and 10, and for the 9° wedge is shown in Figs. 11 and 12, which are the schlieren visualization and the pressure data correspondingly.

Without the plasma, Figures 9(a) to 12(a), the interaction looks consistent with a typical picture: the oblique shock wave is generated due to a supersonic flow interaction with the wedge and then reflects from the top wall. A second shock appears just downstream of the wedge caused by the flow reattachment. When the plasma is switched on a new shock wave is generated from the electrode line on the top wall due to the plasma flow interaction. It is then reflected from the bottom wall (for 3° wedge) or combines with the base shock into a single strong shock (for 9° wedge). The important feature of the SW interaction with the plasma-based displacement layer is that the reflected wedge-based SW is no longer visible or is detected as a very weak compression wave. The pressure measurements prove the effect of the reflected shock mitigation visible on the schlieren images: the pressure peak, caused by an impinging shock wave at about $x=100\text{mm}$, is reduced significantly, as it is shown in Figs. 10(a) and 12(a).

MITIGATION OF REFLECTED SHOCK WAVE BY STREAMWISE PLASMA ARRAY

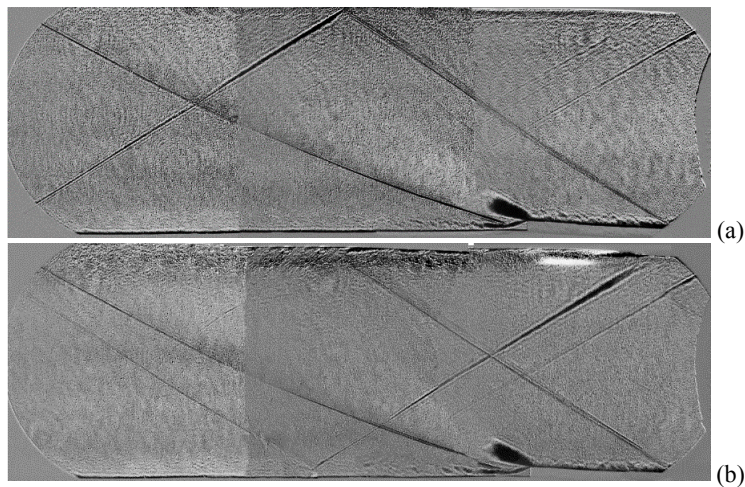


Figure 9. Schlieren image of the interaction of shock wave, originating from a solid 3° wedge on bottom wall, and the shock wave / displacement layer generated by the plasma located on top wall. (a) – plasma off; (b) – plasma on. Flow $M=2$ is from right to left.

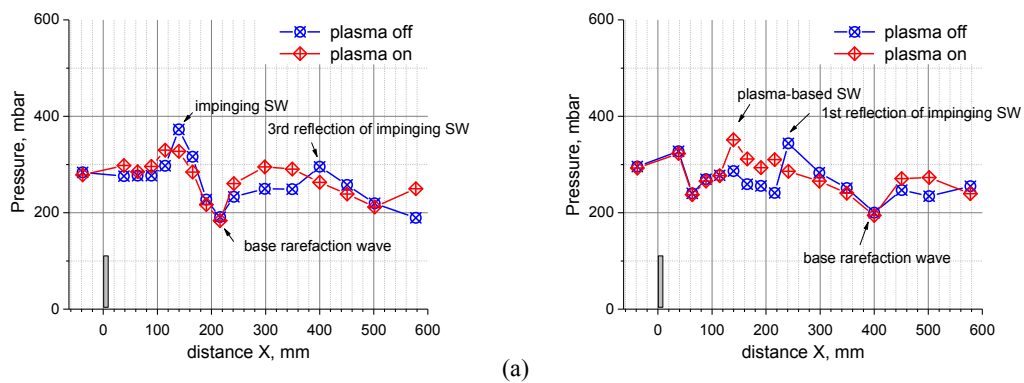


Figure 10. Pressure redistribution over (a) upper wall and (b) bottom wall during plasma generation. Solid 3° wedge on bottom wall.

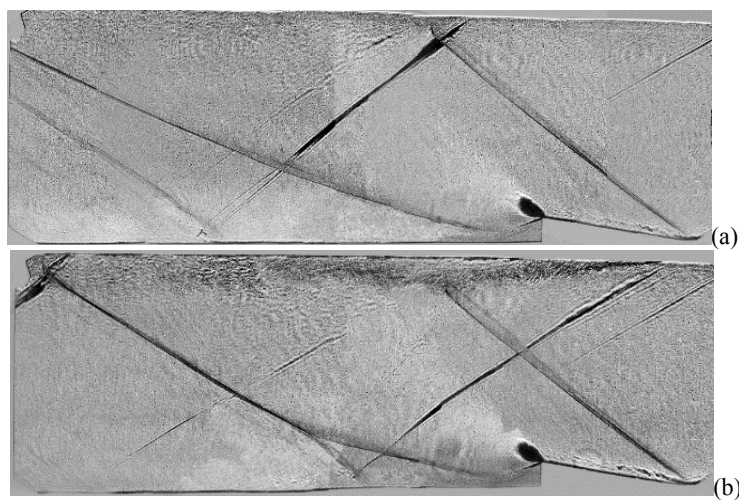


Figure 11. Schlieren image of the interaction of shock wave, originating from a solid 9° wedge on bottom wall, and the shock wave / displacement layer generated by the plasma located on top wall. (a) – plasma off; (b) – plasma on. Flow $M=2$ is from right to left.

Sergey Leonov, Campbell Carter, Alec Houpt, Timothy Ombrello

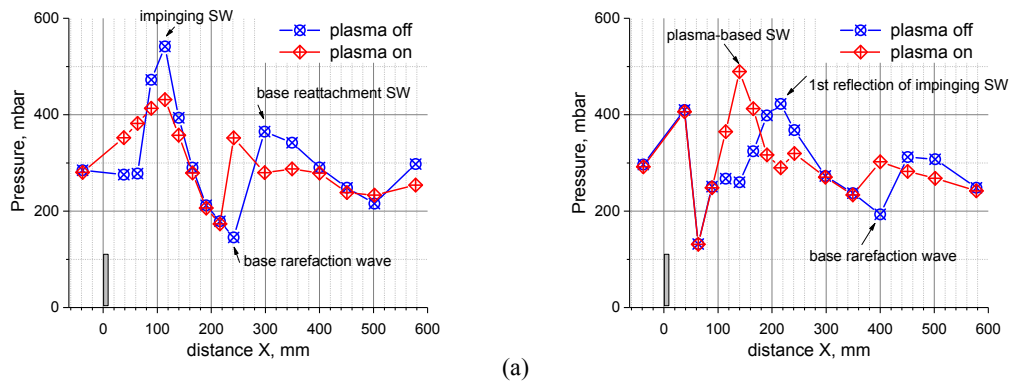


Figure 12. Pressure redistribution over (a) upper wall and (b) bottom wall during plasma generation. Solid 9° wedge on bottom wall.

The pressure measurements also confirm the effect of the pressure elevation in the zone located upstream of the impinging shock wave. This effect of pressure redistribution over the top wall during plasma generation is well-visible in Fig. 12(a). The pressure peak at $x=100$ mm, appearing to be due to the impinging SW reflection, is significantly reduced and “propagated” upstream through the plasma-related subsonic zone, $x < 80$ mm. The result of the interaction is shown in Fig. 11 on the schlieren visualization for plasma off and on, correspondingly. The effect of the reflected shock mitigation or even termination is observed clearly. The shape of the plasma-related wedge complies, as it is shown in Fig. 11(b), reducing the reflected SW strength. The 3rd reflecting SW coming to the same point as the base reattachment SW (impinging SW from the solid wedge reflecting from top wall then from bottom wall and coming to the top wall) is recognizable in Fig. 12(a) at $x \approx 300$ mm if the plasma is off. This SW disappears, being replaced with the plasma-related SW at $x=240$ mm. This is seen even more clearly in Fig. 12(b) at $x=220$ mm and $x=140$ mm correspondingly. The second feature of this type of interaction is that the plasma-related shock wave is “amplified” by the impinging SW due to the pressure augmentation in the zone of plasma filaments, compare the pressure magnitude at $x=140$ mm in Fig. 10(b) and in Fig. 12(b).

4. Discussion and Summary

In fact, the multi-filamentary plasma zone presents a set of longitudinal subsonic jets surrounded by a supersonic flow, as shown in Fig. 13 for a single plasma filament. The volumetrically expanded zone produces a cone of subsonic flow, where the physical velocity may be close to the gas speed in the supersonic core flow. The pressure is increased due to the impact of the impinging SW and affects this cone, increasing the gas pressure in the subsonic zone. The gas expansion induces the conical SW attached to the plasma filament root (electrode). The shape of a “soft” plasma trail complies reducing the reflected SW strength.

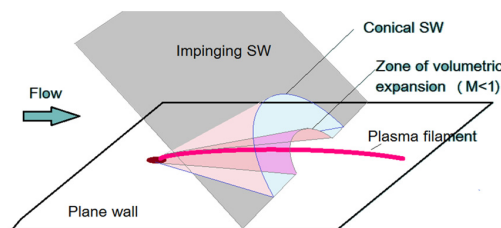


Figure 13. Scheme of a single plasma filament interaction with supersonic flow and impinging shock wave.

In the case of a multi-filament plasma array, shown in Fig. 14, the interference of the conical shock waves produces a combined compression wave attaining the form of a plane shock having a steady shape despite the transient nature of individual plasma filaments. A specific structure of the near-surface gas layer, consisting of the intermittent lengthwise zones of supersonic and subsonic flow, possesses a mitigating effect on an external impinging SW. The mechanism of interaction is considered as follows: the pressure, increasing due to the impact of the impinging SW, affects the whole subsonic area, increasing the gas pressure in the upstream zone and reducing the pressure magnitude right after the SW. This mechanism is confirmed experimentally and considered above in Section 3.

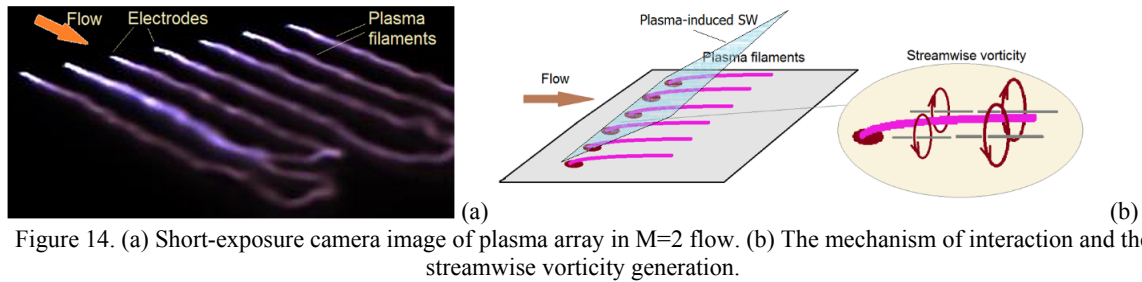


Figure 14. (a) Short-exposure camera image of plasma array in $M=2$ flow. (b) The mechanism of interaction and the streamwise vorticity generation.

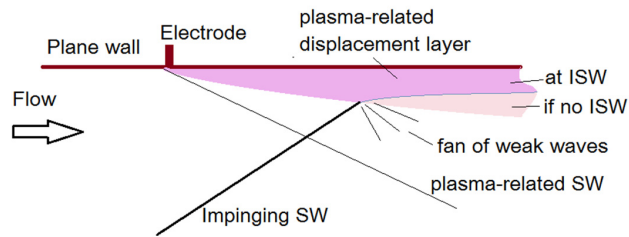


Figure 15. Scheme of active compliant structure generation: a side view at a multiple plasma filament array.

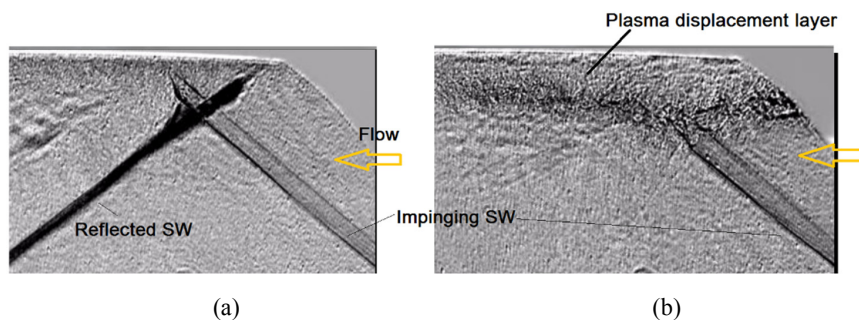


Figure 16. Comparison of the impinging shock reflection pattern (zoomed zone from Fig. 11) without plasma (a) and with filamentary plasma (b). Flow $M=2$, shock is generated by 9° wedge installed on opposite wall.

Figure 15 shows a scheme of interaction of the plasma-based displacement layer with an impinging SW (ISW) resulting in a mitigation effect on the reflected SW. The pressure increase concomitant to the impinging SW is mitigated due to presence of longitudinal subsonic zones, which appears in modification of the shape of the displacement layer, as it is shown in Fig. 16. As a result, the near-wall layer, produced with the help of the longitudinal plasma array, works as a virtual shape or an *active compliant structure*. Such a structure performs in the same way as mechanical compliant structures, which are based on a flexible (membrane) wall construction [35,36]. The plasma-based configuration may potentially be applied to mitigate the reflected SW due to the impinging SW interaction with the plasma-related displacement layer. It is beneficial that the electrical discharge can be switched on/off electronically at any time and synchronized with all other processes, such as a trajectory change or engine thrust modulation. The active compliant structure may aim in shifting the reflected SW, the mitigation of reflected SW strength, or an elimination of the reflected SW for flow control purposes.

Another gasdynamic phenomenon, which is potentially realized during constricted plasma interaction with airflow, is the generation of streamwise vorticity as it is shown schematically in Fig. 14(b). As it was mentioned in early papers of Roth et al [37,38], relatively low-velocity crossflow jets and vortices induced by electrostatic and thermal interaction in DBD discharges may be an effective source of streamwise vorticity. An extensive review of more recent work is given by Jukes and Choi [39] and in a recent papers by Wickes & Thomas and by Moralev [40,17]. It was shown that interaction between the flow in the boundary layer and the plasma-induced body force significantly augments streamwise vorticity, compared to vorticity generated in the absence of an external flow. An array of plasma-based streamwise vortex generators may prevent flow separation by enhancing momentum transfer from the core flow to the boundary layer. For effective production of streamwise vorticity, the near-surface plasma needs to be strongly non-uniform in the spanwise direction. It is important to realize that both the body force and localized heating of the flow can generate streamwise vorticity. Generation of streamwise vorticity in a supersonic flow requires higher power than

is typically realized in DBD actuators. The Q-DC discharge produces high-power longitudinal plasma filaments beneficial for the control of a BL in a compressible flow.

The generation of surface localized discharges in a high-speed flow leads to a substantial change in the structure and parameters of the flow field. The Q-DC electrical discharge affects the flow similar to a *soft* wedge, whose angle depends on the electrical power deposition. The structure of the plasma-based displacement layer appears as an array of intermittent supersonic and subsonic lengthwise zones that is able to effectively mitigate the strength of an impinging external shock wave. To some extent, it works similar to an active compliant structure possessing a feasible potential for the control of shock wave – boundary layer interaction.

Acknowledgments

This work is supported by the AFRL. The construction of SBR-50 facility was funded by the University of Notre Dame.

References

- [1] J Seddon and E L Goldsmith, *Intake Aerodynamics*, 2nd ed.: AIAA Education Series, 1999.
- [2] D. M. VanWie, "Scramjet Inlets. Scramjet Propulsion," in *Progress in Astronautics and Aeronautics*, v.189, E. T. Curran and S. N. B. Murthy, Ed. Reston, VA: AIAA, 2000, ch. 7, pp. 447–511.
- [3] L. E. Surber and J. A. Tinapple, "2012. Inlet Flow Control Technology: Learning from History, Reinventing the Future.," *Paper AIAA 2012-0012*, 2012.
- [4] D. S. Dolling, "Fifty Years of Shock-Wave/Boundary-Layer Interaction Research: What Next?," *AIAA Journal*, vol. 39, no. 8, 2001.
- [5] A. Valdivia, K. B. Yuceil, J. L. Wagner, N. T. Clemens, and D. S. Dolling, "Control of Supersonic Inlet-Isolator Unstart Using Active and Passive Vortex Generators," *AIAA Journal*, vol. 52, no. 6, pp. 1207-1218.
- [6] Yu Wu, Shihe Yi, Lin He, Zhi Chen, and Yangzhu Zhu, "Flow visualization of Mach 3 compression ramp with different upstream boundary layers," *J Vis*, vol. 18, pp. 631-644, 2015.
- [7] S.P. Schneider, "Effects of Roughness on Hypersonic Boundary-Layer Transition," *J. of Spacecraft and Rockets*, vol. 45, no. 2, pp. 193-205, 2008.
- [8] E. Reshotko and A. Tumin, "Role of Transient Growth in Roughness-Induced Transition," *AIAA J.*, vol. 42, no. 4, pp. 766–770, 2004.
- [9] H. Yan and D. Gaitonde, "Effect of Thermally Induced Perturbation in Supersonic Boundary Layers," *Physics of Fluids*, vol. 22, pp. 064101(1-17), 2010.
- [10] A. Fedorov, A. Ryzhov, and V. Soudakov, "Effect of local volume energy supply on high-speed boundary layer stability," *Paper AIAA 2013-2881*, 2013.
- [11] A. Novikov, I. Egorov, and A. Fedorov, "Numerical simulation of three-dimensional wave packet in supersonic flow over a compression corner," *Paper AIAA 2015-2624*.
- [12] Seong-kyun Im et al., "Ramp Separation Response to Laer-Induced Breakdown Disturbed Boundary Layer at M=4.5," *Paper AIAA 2016-0616*.
- [13] R E Hanson, P Lavoie, A M Naguib, and J F Morrison, "Transient growth instability cancelation by a plasma actuator array," *Exp. Fluids*, vol. 49, pp. 1339–48, 2010.
- [14] C. Rethmel et al., "Flow Separation Control Using Nanosecond Pulse Driven DBD Plasma Actuators," *International Journal of Flow Control*, vol. 3, pp. 213-232, 2011.
- [15] A. Kurz et al., "Boundary Layer Transition Control using DBD Plasma Actuators," *Journal AerospaceLab*, vol. 6, 2013.
- [16] V. F. Kopiev et al., "Instability wave control in turbulent jet by plasma actuators," *J Phys D: Appl Phys*, vol. 47, p. 505201, 2014.
- [17] I. Moralev, S. Boytsov, P. Kazansky, and V. Bityurin, "Gas-dynamic disturbances created by surface dielectric barrier discharge in the constricted mode," *Experiments in Fluids*, vol. 55, no. 5, p. 1747, 2014.
- [18] Kwng-So Choi, Timothy Jukes, and Richard Whalley, "Turbulent boundary-layer control with plasma actuators," *Phil. Trans. R. Soc. A*, vol. 369, pp. 1443–1458, 2011.
- [19] S.O. Macheret, M.N. Shneider, and R.B. Miles, "Magnetohydrodynamic and Electrohydrodynamic Control of Hypersonic Flows of Weakly Ionized Plasmas," *AIAA Journal*, vol. 42, no. 11, pp. 1378-1387, 2004.
- [20] M. Samimy et al., "Development and Characterization of Plasma Actuators for High Speed Jet Control," *Experiments in Fluids*, vol. 37, no. 4, pp. 577-588, 2004.

- [21] F. Falempin et al., "Plasma control of shock wave configuration in off-design mode of $M = 2$ inlet," *Experiments in Fluids*, vol. 56, no. 54, 2015.
- [22] M. Samimy, J.-H. Kim, J. Kastner, I. Adamovich, and Y. Utkin, "Active Control of High-speed and High Reynolds Number Jets Using Plasma Actuators," *Journal of Fluid Mechanics*, vol. 578, pp. 305-330, 2007.
- [23] J.-H. Kim et al., "Development of Localized Arc Filament RF Plasma Actuators for High-Speed and High Reynolds Number Flow Control," *Experiments in Fluids*, vol. 49, pp. 497-511, 2010.
- [24] C. Hahn, M. Kearney-Fischer, and M. Samimy, "On factors influencing arc filament plasma actuator performance in control of high speed jets," *Experiments in Fluids*, vol. 51, pp. 591-603, 2011.
- [25] Y. G. Utkin et al., "Development and Use of Localized Arc Filament Plasma Actuators For High-speed Flow Control," *Journal of Physics D: Applied Physics*, vol. 40, pp. 685-694, 2007.
- [26] M. Kearney-Fischer, J.-H. Kim, and M. Samimy, "A Study of Mach Wave Radiation Using Active Control," *Journal of Fluid Mechanics*, vol. 681, pp. 261-292, 2011.
- [27] M. Nishihara, K. Frederickson, and W. R. Lempert, "Dual-Pump CARS Measurements in a Vibrationally Nonequilibrium Supersonic Mixing Layer," *Paper AIAA 2016-1762*.
- [28] S. B. Leonov and D. A. Yarantsev, "Control of separation phenomena in high-speed flow by means of the surface electric discharge," *Fluid Dynamics*, vol. 43, no. 6, pp. 945-953, 2008.
- [29] B. Hedlund, A. Houpt, T. Ombrello, and S. Leonov, "Controllable Shock Wave Generation by Near-Surface Electrical Discharge," *AIAA Paper 2016-4306*, 2016.
- [30] M. N. Shneider, S. O. Macheret, S. H. Zaidi, I. Girgis, and R. B. Miles, "Virtual Shapes in Supersonic Flow Control with Energy Addition," *Journal of Propulsion and Power*, vol. 24, no. 5, pp. 900-915, 2008.
- [31] S. B. Leonov and D. A. Yarantsev, "Near Surface Electrical Discharge in Supersonic Airflow: Properties and Flow Control," *Journal of Propulsion and Power*, vol. 24, no. 6, pp. 1168-1181, 2008.
- [32] A. Houpt, B. Hedlund, T. Ombrello, C. Carter, and S. Leonov, "Quasi-DC Electrical Discharge Characterization in a Supersonic Flow," *Experiments in Fluids*, vol. 58, no. 4, 2017.
- [33] I.V. Nemchinov et al., "Rearrangement of the bow shock shape using a "hot spike" ," *Shock Waves*, vol. 4, pp. 35-40, 1994.
- [34] P.Y. Georgievskiy and V.A. Levin, "Front separation regions for blunt and streamlined bodies initiated by temperature wake – bow shock wave interaction," in *Hannemann K., Seiler F. (eds) Shock Waves. Springer, Berlin, Heidelberg, 2009*, pp. 1273-1278.
- [35] Z. B. Riley, J. J. McNamara, and H. B. Johnson, "Assessing Hypersonic Boundary-Layer Stability in the Presence of Structural Deformation ," *AIAA JOURNAL*, vol. 52, no. 11, 2014.
- [36] D. Bountin, T. Chimitov, and A. Maslov, "Stabilization of a Hypersonic Boundary Layer Using a Wavy Surface," *AIAA Journal*, vol. 51, no. 5, pp. 1203–1210, 2013.
- [37] J. R. Roth, D. M. Sherman, and S. P. Wilkinson, "Electrohydrodynamic Flow Control with a Glow Discharge Surface Plasma," *AIAA Journal*, vol. 38, no. 7, pp. 1166- 1172, 2000.
- [38] J R Roth, D M Sherman, and S P Wilkinson, "Boundary layer flow control with a one atmosphere uniform glow discharge surface plasma," *AIAA paper 1998-0328*, p. AIAA Meeting (Reno USA January 1998) , 1998.
- [39] T. N. Jukes and Kwing-So Choi, "On the formation of streamwise vortices by plasma vortex generators," *J. Fluid Mech.*, vol. 733, pp. 370-393, 2013.
- [40] M. Wicks, F. O. Thomas, T. C. Corke, M. Patel, and A. B. Cain, "Mechanism of Vorticity Generation in Plasma Streamwise Vortex Generators," *AIAA Journal*, vol. 53, pp. 3404-3413, 2015.